Multiphase equation of state and elastic moduli of solid beryllium from first principles

G. Robert,* P. Legrand, and S. Bernard
CEA, DAM, DIF, F-91297 Arpajon Cedex, France

(Received 22 December 2009; revised manuscript received 10 June 2010; published 27 September 2010)

Based on *ab initio* calculations, we provide a consistent modeling in pressure and temperature of the solid phases of beryllium, including theoretical phase diagram, multiphase equation of state (EOS), and elastic moduli. The quasiharmonic approximation (QHA) allows us to determine the whole theoretical phase diagram: at room temperature, QHA predicts the hexagonal compact (α-hcp) phase as the most stable structure up to 400 GPa, where a transition toward the body-centered-cubic (β-bcc) phase occurs. However, the QHA does not account for the low-pressure-high-temperature bcc phase found experimentally. Combining frozen phonon and density-functional perturbation theory methods, we show that soft phonon modes as reservoirs of entropy may stabilize the low-pressure bcc phase. However the thermodynamic stability of this phase has still to be established. We provide the QHA multiphase EOS in analytic form and an evaluation of the uncertainties on the QHA solid-solid and solid-liquid phase boundaries. Then, we calculate the density and temperature dependence of elastic constants by determining the free energies of strained structures. Consistency between the polycrystalline (i.e., averaged over the elastic constants) and the EOS isothermal bulk moduli is achieved for both phases. Our results are in fair agreement with the most recent experimental data and permit us to raise questions on some experimental moduli.

DOI: 10.1103/PhysRevB.82.104118 PACS number(s): 64.30.Ef, 31.15.A−, 62.20.de

I. INTRODUCTION

Beryllium, although a "simple" metal with "only" four electrons remains a challenge for both theory and experiment, even if considerable work has been recently published on the subject. Indeed, it is an important element for nuclear power industry, for aeronautics, and it has been considered as a possible ablator material for fuel capsules in inertial confinement fusion experiments. For those various applications, where beryllium structures experience various kinds of static and dynamic loading,[1] one needs a consistent and hopefully predictive model of the material, including equation of state (EOS) and strength.

Beryllium is a tough candidate for first-principles calculations, mainly due to the fact that there are several competing phases in the solid part of the phase diagram that are very close in energy, so the transition lines are extremely sensitive to the numerical quality of the calculations. The aim of this paper is thus to present a unified picture of the multiphase EOS and elastic moduli of solid Be obtained through a fully *ab initio* approach. We will, in particular, try to shed some light on a controversial issue concerning the phase diagram at low pressure and high temperature and on the thermoelastic properties along the 1 bar isobar.

According to handbooks,[2] the room-temperature-room pressure (RT-RP) stable phase of beryllium is hexagonal compact (hcp: α-Be); at room pressure and 1530 ± 10 K, it transforms into a body-centered-cubic (bcc: β-Be) phase which melts at 1560 K. However, the very existence of this phase, its stability domain, and of course the behavior of the α-β transition under pressure, are not clearly established and some experimental results are hardly compatible. For example, according to,[3–6] the α-β phase line has been observed (up to 6GPa) to decrease with increasing pressure with a slope of -52 ± 8 K/GPa and a density increase at the transition on the order of 3.5–4.5 %. On the contrary, Abey[7] found a slope of 43 ± 7 K/GPa up to 0.6 GPa with a density decrease of 4.8%. In this last case, the α-β phase line should not cross the 300 K isotherm whereas, in the first case, by linear extrapolation it should cross it around 21 GPa. There has been a serious experimental effort to locate this transition at room temperature using diamond anvil cells (DAC). Ming and Manghnani[8] observed a slightly distorted hcp phase at pressures between 8.6 and 14.5 GPa (reinterpreted by Vijayakumar *et al.*[9] as an orthorhombic cell with four atoms). However, most experimentalists do not detect any kind of phase transition up to 180 GPa.[10–13] In temperature, Evans *et al.* as quoted in Ref. 14, failed to find any evidence for a phase transition between 15 and 50 GPa up to 2000 K in DAC. Moreover, shock data up to 35 GPa do not exhibit any evidence of an hcp-bcc transition along the Hugoniot.[15]

As regards elastic properties, the elastic constants at RP have been measured at room temperature,[16,17] from 0 K to RT (Refs. 18 and 19) and from RT up to ~1000 K.[20,21] However, the temperature dependence of the bulk and shear moduli deduced from low-temperature (below RT) and high-temperature (from RT to 1000 K) measurements shows large discrepancies.

First-principles calculations are widely used to elucidate that kind of experimental dilemma and to explore the domain where data are necessary but difficult to obtain through experiment. In the past few years, the equation of state and elastic constants of beryllium have been subject to several first-principles studies within density-functional theory.[14,22–24] Part of our own contribution to this theme has already been published elsewhere.[25–27]

In this paper, we present a comprehensive view of our calculations and concentrate on phonon calculations and on their contributions to the comprehension of the physics of beryllium. It is well known[28] that to determine a transition pressure at 0 K, one has to take into account the difference of zero-point energies between the competing phases which may be crucial. As for the thermal part of the EOS, all the

quasiharmonic thermodynamic information is contained in just a few of the moments of the phonon density of states (PDOS). The QHA is frequently reduced to the quasiharmonic conventional Debye model (QHCDM), in which all the moments of the PDOS are supposed to be equal, and this unique moment is then extracted from elastic-constant calculations. The QHCDM is not valid for beryllium, so the PDOS has to be calculated for each phase.

As for the presence of a low-pressure β-bcc phase below the melt curve, calculations based on QHCDM (Refs. 22 and 23) predict it whereas those based on more reliable QHA do not.[14] Of course, both, by construction, do not take into account anharmonicity. Theoretically, the bcc structure is found to be dynamically unstable at 0 K and low densities due to imaginary frequencies of the T_1 mode in Γ-N direction. Soft phonon modes as reservoirs of entropy may stabilize this phase in temperature, but the evolution of this mode with temperature has not been studied.[14] We address this point by combining density-functional perturbation theory (DFPT) and frozen phonons methods.

Phonon calculations are also useful to obtain the behavior of elastic constants as a function of temperature along isochors,[29] and thus provide, after appropriate polycrystalline averages, the evolution of macroscopic elastic moduli with density ρ and temperature T.

This paper is arranged as follows: part II is devoted to a discussion of our first-principles calculations, with a particular focus on the full *ab initio* phonon densities of state of the hcp and bcc phases and their connection to the hcp to bcc transition line, zero-point energy and multiphase EOS in a quasiharmonic framework. The stability at low pressure and high temperature of the bcc phase, which does not exist within QHA due to an imaginary phonon mode, is addressed by calculating the temperature dependence of this mode.

Part III presents the QHA validity domain for the solid phases, bounded by our QMD melt curve calculations and by the possible low-pressure-high-temperature bcc phase. Part IV provides the QHA multiphase EOS in analytic form and an evaluation of the uncertainties on the phase boundaries.

Part V deals with elastic-constants calculation as a function of pressure and temperature within DFPT. From these, after averaging, we propose coefficients for an analytic form of polycrystalline bulk and shear moduli, suitable for constitutive models for hydrocodes and assess critically experimental values. The computational details can be found in Appendix.

II. LATTICE DYNAMICS

First of all, we have to determine which phases should appear in the phase diagram. Apart from the usual hcp, bcc, and face-centered-cubic (fcc) structures, we have also checked structures which may appear in a hcp to bcc martensitic transformation (or one of its variants):[30] the orthorhombic α-U-type structure (proposed in Ref. 9 and already rejected in Ref. 31) or the rhombohedral α-Sm type. The corresponding ground-state energies relative to the hcp phase without zero-point contribution are presented in Fig. 1.

Depending on density, the α-U structure relaxes either into hcp or bcc structure. In the ground state, the α-Sm type and fcc structures are never energetically stable, even if we take into account zero-point correction and ionic contribution to the free energy (not shown here).

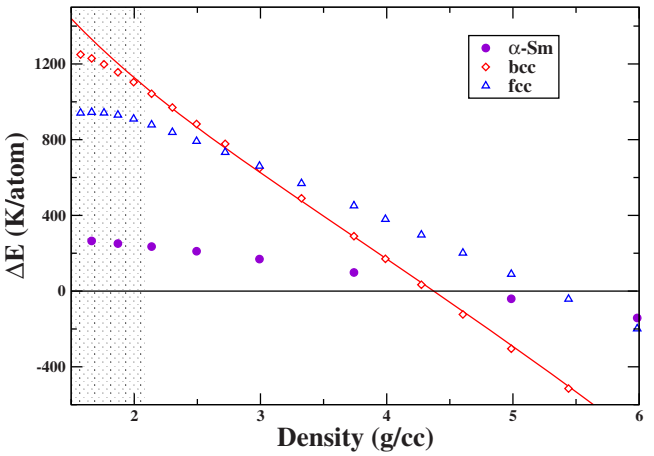

FIG. 1. (Color online) Energies differences (in kelvin) of fcc, bcc, and α-Sm structures versus hcp Be in the ground state as function of density. The zero-point contribution is not taken into account. The full red line reproduces the energy differences between bcc and hcp after fit (see Table II). Grey zone indicates the regime where the bcc phase is dynamically unstable in the ground state according to DFPT ($\rho < 2.1$ g/cc, see below).

Subsequently, we will concentrate here on the hcp and the bcc phases and only the phonon curves and densities of states for these two phases are detailed.

A. Hexagonal compact structure phonons

Figure 2 shows the calculated phonon-dispersion relations, compared to the experimental neutron-scattering data at 80 K and ambient pressure ($\rho = 1.854$ g/cc which corresponds to our ground-state equilibrium density).[32] The discrepancy is less than 3% for all high-symmetry points. The hcp dispersion curves from 1.4 g/cc to 6 g/cc do not show any anomaly or instability.

Such phonon-dispersion relations permit us to determine the ion-vibrational term of the harmonic free energy F_H

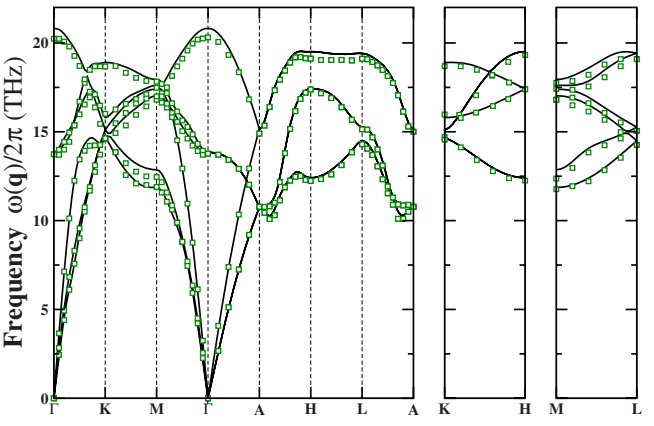

FIG. 2. (Color online) Phonon-dispersion relations of hcp Be from our calculations at 1.87 g/cc (full lines) compared with 80 K neutron-scattering data at 1.854 g/cc (squares) (Ref. 32).

$$F_H(\rho,T) = 3N\int_0^\infty \left[\frac{1}{2}\hbar\omega + k_B T \ln(1-e^{-\hbar\omega/k_B T})\right] g(\rho,\omega)d\omega, \tag{1}$$

where ω are the phonon frequencies and $g(\rho,\omega)$ is the normalized PDOS at density ρ. The quasiharmonic phonon frequencies depend on density but not on temperature.

It is sometimes meaningful to discuss not all the PDOS but only a few phonon characteristic temperatures θ_n which correspond to different moments of the PDOS (Ref. 33)

$$\ln(k\theta_0) = \langle \ln(\hbar\omega)\rangle_{BZ}; \quad k\theta_1 = \frac{4}{3}\langle \hbar\omega\rangle_{BZ};$$

$$k\theta_2 = \left[\frac{5}{3}\langle(\hbar\omega)^2\rangle_{BZ}\right]^{1/2}, \tag{2}$$

where $\langle\cdots\rangle_{BZ}$ indicates a Brillouin zone average (θ_0 is the logarithmic moment, θ_2 is related to the root-mean-square average of phonon frequencies).

Another useful data is the well-known Debye temperature, which depends on the acoustic phonon velocities and is defined by the $n=-3$ moment of the PDOS

$$k\theta = k\theta_{-3} = \lim_{n\to -3}\left[\frac{n+3}{n}\langle(\hbar\omega)^n\rangle\right]^{1/n}. \tag{3}$$

Throughout this paper, the $n=-3$ moment is obtained by calculating the average sound velocity c_s from elastic constants[33] as explained in detail in Ref. 34 in order to avoid the limit problem in Eq. (3)

$$k_B\theta_{-3} = \hbar c_S\left(\frac{6\pi^2\rho}{M}\right)^{1/3}, \tag{4}$$

where M is the mass, $\hbar$ and k_B are Planck and Boltzmann constants.

Each moment can be related to distinct thermal properties (Table VI.1 in Ref. 33). For example, the $n=-3$ corresponds to low-temperature properties, $n=1$ zero-point correction, and $n=0$ entropy at high temperature.

Debye characteristic temperatures for $n=-3$, 0, 1, and 2 are plotted in Fig. 3. We find that, at each density, all moments are nearly equal but the $n=-3$ (diamonds in Fig. 3) moment, for which the departure from the other moments is large. Our results are consistent with other theoretical works,[14,24] and, as already said, rule out the use of QHCDM for beryllium.

Some characteristic Debye temperatures have experimental counterparts.[33] We find thus a good agreement between experimental Debye temperature deduced from low-temperature specific-heat and elastic-constants measurements up to 300 K: 1465 ± 25 K (Refs. 16, 18, and 35–37) and $\theta_{-3}=1475$ K (upper red circle with error bar in Fig. 3). The calculated characteristic Debye temperature for $n=2$ which corresponds to high-temperature behavior is 935 K (stars in Fig. 3) and also compares favorably with experimental values of 949 ± 51 K (Refs. 35, 36, and 38–40) (lower red circle with error bar in Fig. 3).

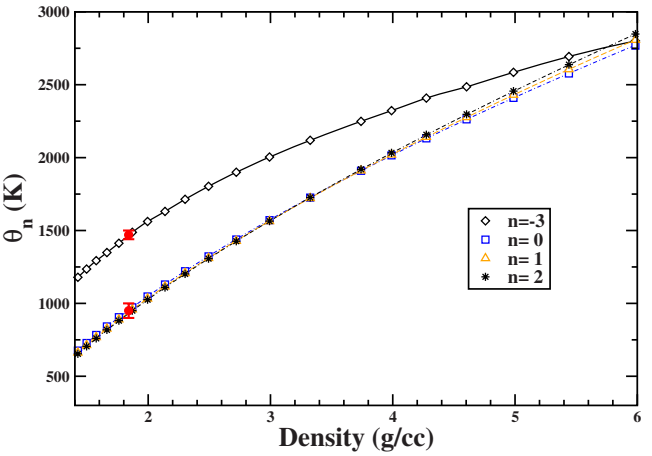

FIG. 3. (Color online) Calculated θ_n for hcp structure at different densities. Dashed lines reproduce the fit in Table III. For $n=-3$, full line is a spline interpolation between raw calculated points. Full circles show the experimental values from elastic and heat-capacity measurements (see text for references).

B. Body-centered-cubic structure phonons

Contrarily to the hcp phase, the bcc dispersion curves show anomalous features at low density. For example, the phonon-dispersion relations corresponding to two densities are plotted in Fig. 4.

As density decreases, the phonon frequency of the T_1 mode along the Γ-N direction decreases and becomes imaginary below 2.1 g/cc, and thus, below this density, the bcc structure becomes dynamically unstable. This is apparently in contradiction with the stability of the bcc phase at nearly RP and high temperatures evidenced experimentally where the equilibrium density of bcc phase is around 1.8 g/cc. We will address this issue in the next section.

Figure 5 shows the characteristic Debye temperatures obtained from these calculations. The $n=-3$ Debye temperature (diamonds in Fig. 5) is 1066 K at $\rho=1.918$ g/cc (which corresponds to our ground-state equilibrium density) close to previously published results ($\theta_{-3}=1045$ K,[23] θ_{-3}

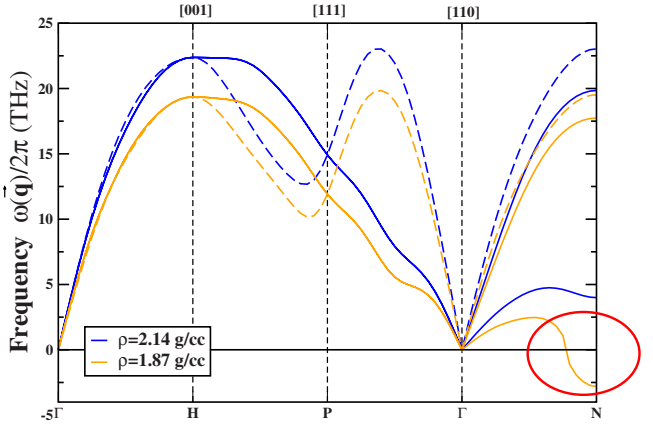

FIG. 4. (Color online) Phonon-dispersion relations of bcc Be from our calculations for two different densities. Circle points out imaginary frequencies. Upper curves reproduce frequencies for $\rho=2.14$ g/cc.

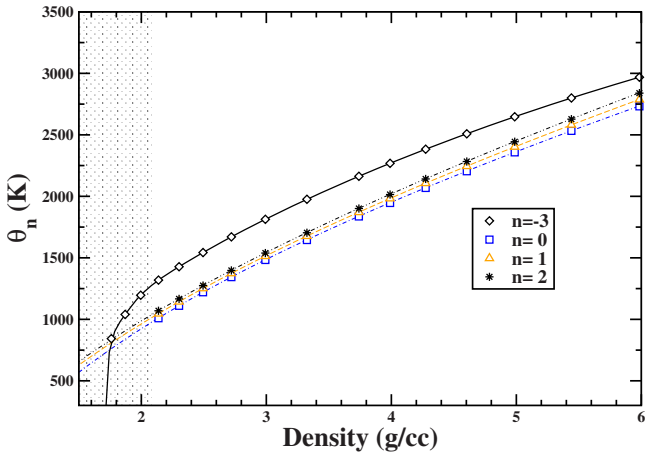

FIG. 5. (Color online) Calculated θ_n for bcc structure at different densities. Dashed lines reproduce in parameter reported in Table IV. For $n=-3$, full line is a spline between raw calculated points. The gray zone indicates the domain of dynamical instability of bcc phase in the ground state obtained within DFPT ($\rho<2.1$ g/cc).

$=1086$ K;[28] only in Ref. 22 is a somewhat higher value to be found $\theta_{-3}=1217$ K). Like for the hcp phase, for each density, the characteristic Debye temperatures difference for all moments (squares, triangles, and stars in Fig. 5) is within 50 K except for $n=-3$ where it reaches 300 K.

Due to the dynamic instability, a QHA model for the bcc phase is only valid for densities greater than 2.1 g/cc. Therefore, the low-pressure-high-temperature β phase seen experimentally cannot be addressed in this framework.

As we already noted the QHCDM cannot be used for Be. Thus, if both phase diagrams predicted using this model[22,23] match the experimental phase diagram, it should only be fortuitous. One more precision: Kádas *et al.*[22] claim that the β phase should be destabilized below $\rho\approx 1.8$ g/cc due to an electronic topological transition, which would lead to a softening of the elastic constants (thus θ_{-3}) and thus to the violation of Born criterion. This picture is inconsistent with both our work[25] and Benedict *et al.*[14] study based on full dispersion curves. If Born criterion is violated only below 1.8 g/cc, the dynamical instability of T_1 mode at N point persists up to 2.1 g/cc. To try to address the conditions of existence of the bcc phase (below 2.1 g/cc) from a qualitative point of view but on the same theoretical footing as the rest of this paper, we have studied the evolution of the T_1 mode at N point with temperature to check the possibility that the bcc phase be stabilized by temperature at low pressure.

C. Evolution of the T_1 phonon mode at N point with density and temperature: possible existence of a β-bcc phase at low pressure below the melt curve

To quantify accurately anharmonic effects within first-principles calculations remains a real challenge. However, we may address the evolution of the frequency of the T_1 mode at N point with temperature. According to the frozen phonon method, using a supercell and applying an appropriate atomic displacement $\boldsymbol{u}(\boldsymbol{\lambda})$, we access the corresponding frequency mode. At fixed density and temperature, the

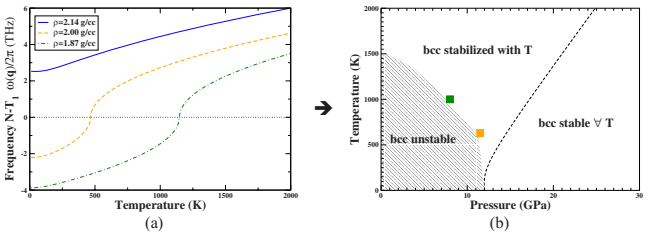

FIG. 6. (Color online) (a) Evolution in temperature of frequency at the N-point of the T_1 phonon mode for three isochors. (b) Possible existence domain of the bcc phase in low pressure due to anharmonic effects. Squares reproduce the estimated pressure-temperature stability of the bcc phase determine by our procedure: the color code is the same in the two figures.

square of the frequency at the corresponding high-symmetry point (in our case the N point) is proportional to the second derivative of the free energy with respect to displacement λ

$$\omega_N^2(\rho,T) \propto \partial^2 F_{tot}(\rho,\lambda,T)/\partial\lambda^2. \tag{5}$$

So, for each displacement, we perform DFPT on the supercell.[41] The phonon dispersion curves are calculated and the PDOS is extracted in order to obtain Helmholtz free energy within the full quasiharmonic approximation for the supercell (see Appendix for more details).

We then have

$$F_{tot}(\rho,\lambda,T) = E(\rho,\lambda,0) + 3N\int_0^\infty \left[\frac{1}{2}\hbar\omega + k_B T \ln(1-e^{-\hbar\omega/k_B T})\right] \times g(\rho,\lambda,\omega)d\omega, \tag{6}$$

where ω are the corresponding phonon frequencies and $g(\rho,\lambda,\omega)$ is the normalized PDOS for displacement λ.

Obviously, expression in Eq. (6) only holds for real frequencies. Here, we have to deal with imaginary frequencies which can remain in the low-frequency part of the phonon-dispersion spectrum of the supercell. Usually, to get rid of imaginary frequencies in the full phonon spectrum and provide a suitable expression for the free energy, one sets them to zero and renormalizes the PDOS. We have chosen here to define a less arbitrary renormalization procedure. We impose, by acting on the low-frequency part of the PDOS (<3 THz), that the pressure calculated as the volume derivative of Eq. (6) matches the QMD pressure obtained for the same densities and temperatures.[26]

Both renormalizations affect in a slightly different way the entropy which is responsible of the rising up of the frequency in temperature. However, only the last one allows us to switch consistently with respect to QMD pressure between ω-T and p-T representations along an isochor.

Results obtained by this procedure are reproduced in Fig. 6(a) for three isochors. For the 2.14 g/cc isochor, the frequency of the T_1 mode at N point is roughly unaffected by temperature. So we can consider that for densities above 2.1 g/cc and for temperature slightly above the Debye temperature the QHA is valid.

TABLE I. Parameters of the melt curve as defined by Eq. (7).

ρ_0 (g/cc)	$T_m(\rho_0)$ (K)	ξ_1 $[(g/cc)^{1/3}]$	ξ_2 $[(g/cc)^q]$	q
1.72	1560	0.12	3.13	2.053

On the contrary, for $\rho=2$ g/cc and 1.87 g/cc, there is a strong evolution: the imaginary frequencies disappear above 500 K and 1100 K, respectively [Fig. 6(a)]. According to our procedure, these frequency-temperature points correspond to pressures of 12 GPa and 8 GPa, respectively [Fig. 6(b)]. This suggests that in this regime, anharmonic effects are important.

We can define two distinct regimes roughly delimited by the line going through theses points. Below this line, the frequency of the T_1 mode at N point remains imaginary and it becomes real above.

So, by estimating the evolution of the frequency of the T_1 mode at N point with temperature, we have shown that the bcc structure could be dynamically and mechanically stable at low pressure and high temperature.

However to prove that it has the lowest Gibbs free energy compared to hcp is beyond the scope of these calculations below 2.1 g/cc. Should it be the case, to be consistent with recent heated DAC experiments by Evans *et al.* cited in Refs. 14 and 42 which report no experimental evidence of a bcc phase between 15 and 50 GPa up to 2000 K, its maximum pressure stability should be lower than 15 GPa.

III. QUASIHARMONIC SOLID PHASES BOUNDARIES

In order to bound the solid phases domain, we consider the melt curve that we previously calculated by a quantum molecular dynamics "heat until melts" (HUM) technique, which is generally considered as an upper bound of the real melt curve (already discussed in Ref. 26).

In the case of Be, HUM seems to give reasonable agreement with the more predictive two phase's coexistence approach.[14] As our QMD calculations give the same slope (within numerical uncertainties) for the melt curve, whatever the solid phase considered, we define a single melt curve for the two solids.

We fit the QMD melt curve through the following expression:[43]

$$T_m(\rho) = T_m(\rho_0)\left(\frac{\rho}{\rho_0}\right)^{1/3} \exp\left[-6\xi_1(\rho^{-1/3}-\rho_0^{-1/3}) - \frac{2\xi_2}{q}(\rho^{-q}-\rho_0^{-q})\right]. \quad (7)$$

This formulation matches very well the corresponding raw QMD points. We used as reference value the experimental value for $T_m(\rho_0)$ and the corresponding density obtained through our hcp quasiharmonic EOS (see part IV). All the parameters are given in Table I.

We would like to stress here that most of the analytic formulas that we use are from Ref. 43 where they are part of a consistent model, the so-called Burakovsky model. We only use them here as convenient analytic forms.

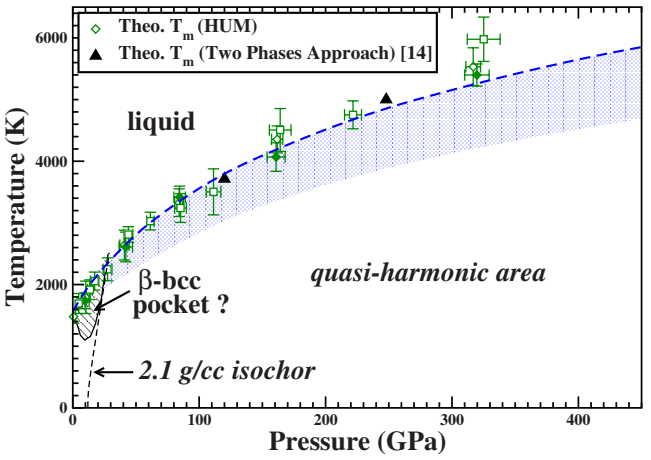

FIG. 7. (Color online) Theoretical solid-liquid domain. Solid domain is divided into two parts: one where quasiharmonic approximation is sufficient to treat correctly the solid, i.e., hcp and bcc above 2.1 g/cc isochor (dashed line); a low pressure β-bcc pocket stabilized by anharmonic effects (see text). The empty diamonds, full diamonds, and empty squares are the *ab initio* melting curve obtained by HUM technique from fcc, hcp, and bcc phases, respectively, and full triangles by two phases approach method (Ref. 14). The gray part below melting curve reproduces the classical admitted uncertainties created by use of HUM method.

With the previous discussion on the N-T_1 high-symmetry points, we can estimate the quasiharmonic phase boundaries and Fig. 7 summarizes these results.

(1) Below 2.1 g/cc, the thermal properties of the bcc phase are driven by anharmonic effects which could stabilize it with respect to the free energy of the hcp phase. If it is the case, a pocket of bcc phase would exist.

(2) Due to high Debye temperature, QHA seems to be reasonable in the whole hcp solid range and above 2.1 g/cc for the bcc phase. Close to the melting curve, strong anharmonic effects could occur. However pressures obtained from QHA compare well with direct QMD calculations used to determine $T_m(\rho)$ which seems to indicate that anharmonic effects are not too strong, in agreement with Benedict *et al.*[14]

(3) The melt curve is reproduced by the dashed line. We also illustrate by a shaded area the region where the melt curve could take place assuming a 20% overestimate of the HUM melt curve.[44,45]

IV. PHASE DIAGRAM AND QHA-EOS

In a multiphase material, each phase has its own crystal structure and properties. Yet, the theoretical description of the free energy of each phase is universal in form.

Neglecting electron-phonon coupling, the Helmholtz free energy $F(\rho,T)$ is given by

$$F(\rho,T) = \Phi_0(\rho) + F_E(\rho,T) + F_I(\rho,T), \quad (8)$$

where $\Phi_0(\rho)$ is the static lattice potential, $F_I(\rho,T)$ is the ion-vibrational free energy, and $F_E(\rho,T)$ is the contribution due

TABLE II. Parameters of Eqs. (9) and (10): a_1, a_2 are in (eV/at); a_3 in [eV(g/cc)$^{-1/3}$/at]; and a_4 in (g/cc)$^{-1/3}$. a_0^e is in states eV^{-1}(g/cc)$^{2/3}$.

Structure	a_1	a_2	a_3	a_4	a_0^e
hcp	124.7664	−501.6522	99.2157	0.2617844	0.0955
bcc	198.1521	−574.3426	108.1086	0.2457026	0.1693

to thermal excitation of the electrons from their ground states.

We now turn to the practical construction of our analytical equation of state in the QHA. For each phase, we represent the static lattice energy with the following form:

$$\Phi_0(\rho) = a_1 + (a_2 + a_3\rho^{1/3})\exp(a_4\rho^{1/3}). \quad (9)$$

This formula gives a very small difference on the whole studied domain between raw and fitted data (see difference between symbols and full lines in Fig. 1).

For both phases, the electron thermal contribution can be expressed within a conventional Sommerfeld model which is a sufficient approximation as long as only the solid phases are concerned.

$$F_E(\rho,T) = -\frac{\pi}{6}n_F(\rho)T^2 = -\frac{\pi}{6}a_0^e\rho^{-2/3}T^2. \quad (10)$$

The parameters for Eqs. (9) and (10) are provided in Table II.

From expansion of Eq. (1) in terms of PDOS moments, the ionic contribution to the Helmholtz free energy can be written as

$$F_I(\rho,T) = \frac{9}{8}k_B\theta_1(\rho) + 3k_BTD_e[\theta_0(\rho)/T] - 3k_BT\left\{\frac{4}{3}D_e[\theta_0(\rho)/T] - \ln(1-e^{-\theta_0(\rho)/T})\right\}, \quad (11)$$

where D_e is the normalized Debye integral. Except for the low-temperature range (T below few kelvins), difference in ionic contributions given by Eqs. (1) and (11) are well below the numerical imprecision due to the analytic model (estimated as a few kelvins, see below).

In order to build an analytical EOS we need an analytic form for the ion thermal contribution and so we need to interpolate the $n=0$ and $n=1$ PDOS moments and differentiate them to obtain thermodynamic functions. We adopt the analytical form suggested by Burakovsky and Preston[43]

$$\theta_n(\rho) = \theta_n(\rho_0)\left(\frac{\rho}{\rho_0}\right)^{1/2}\exp\left[-3\gamma_1(\rho^{-1/3}-\rho_0^{-1/3}) - \frac{\gamma_2}{q}(\rho^{-q}-\rho_0^{-q})\right]. \quad (12)$$

The coefficients γ_1, γ_2, and q for moments $n=0$ and 1 are reported in Tables III and IV. The ρ_0 for the hcp and the bcc structures are taken from our calculations in the ground state (1.889 g/cc and 1.918 g/cc, respectively). For the bcc phase, the fit is only based on values in its stability domain (i.e., $\rho > 2.1$ g/cc). The fitted Debye characteristic temperatures are plotted in Figs. 3 and 5 in dashed lines.

Figure 8 shows the resulting QHA phase diagram. For the solid phases, we estimate the uncertainties on our fits and on *ab initio* raw data to be on the order of 0.5% on θ_D and $F_E(\rho,T)$ and 0.5 meV/atom on the cold curve. These moderate uncertainties can affect the phase diagram (gray part in Fig. 8) as already underlined by Benedict *et al.*[14] We must underline that, from free energy within QHA, the bcc phase never appears below 70 GPa for $T < T_m$.

V. ELASTIC PROPERTIES

Once the equation of state is fixed, the following step toward a consistent model of the material for hydrocodes is to provide a so-called constitutive law, which deals with the elastic-plastic behavior. A full first-principles approach is not of order in this domain, and most of the time, one has to use a more or less empirical model, the parameters of which are fitted on experiment at (relatively) low deformations and deformation rates. However, an important input for such models is the pressure and temperature evolution of the elastic moduli (e.g., shear and bulk) of the polycrystalline material. These quantities can be related, through some approximations (polycrystalline averages) to the individual elastic constants of the material which can be calculated *ab initio*.

A. Elastic properties from *ab initio* calculations

To calculate the evolution of elastic constants with pressure and temperature, we have classically applied the so-called deformations method. Each structure is distorted according to different strains, parametrized by a single parameter δ. The internal stress of each strained structure is removed in the ground state by relaxation of the internal degrees of freedom. We then calculate the PDOS of each strained structure, in order to obtain the value of the Helmholtz free energy.

TABLE III. Parameters of Eq. (12) for the hcp phase. θ_n (K), γ_1 (g$^{1/3}$/cm), γ_2 (g^q/cm^{3q}), and q without unit.

	hcp (ρ_0=1.889 g/cc)	
	$n=0$	$n=1$
$\theta_n(\rho_0)$	984	969
γ_1	0.4239	0.4817
γ_2	1.4762	1.4887
q	2.3579	2.5003

TABLE IV. Parameters of Eq. (12) for the bcc phase. θ_n (K), γ_1 ($g^{1/3}/cm$), γ_2 (g^q/cm^{3q}), and q without unit.

	bcc (ρ_0=1.918 g/cc)	
	n=0	n=1
$\Theta_n(\rho_0)$	870	911
γ_1	0.4852	0.4917
γ_2	3.2677	2.0492
q	2.6598	2.3576

The difference, ΔF, between the Helmholtz free energies [as defined in Eq. (1)] of the distorted and the perfect lattice is fitted with a fourth-order polynomial form as a function of δ and then equated to the appropriate isothermal elastic-constant expression according to Barron and Klein[46] (see Appendix).

The expression for strain-energy density is[46]

$$\frac{\Delta F}{V} = -p\varepsilon_{ii} + \frac{1}{2}\left[c_{ijkl} - \frac{1}{2}p(2\delta_{ij}\delta_{kl} - \delta_{il}\delta_{jk} - \delta_{jl}\delta_{ik})\right]\varepsilon_{ij}\varepsilon_{kl}, \tag{13}$$

where δ_{ij} is the Kronecker delta, ε_{ij} the strain components, and c_{ijkl} are calculated elastic constants.

Figure 9 shows the individual isothermal elastic constant c_{ij}^T along the RP isobar that we extracted from the previous calculations, by using the thermal expansion of our EOS (full line) together with the experimental adiabatic elastic constant c_{ij}^S (symbols).

At RT-RP, compared to Migliori *et al.*[18] experimental data, our calculations reproduce the principal diagonal of the c_{ij} matrix and show a weak departure from them for the off-diagonal terms (triangles up in Fig. 9). Except for c_{11} and to a lesser extend for c_{44}, experimental elastic constants show a gap between low-temperature measurements of Smith and Arbogast[19] (yellow diamonds) and high-temperature measurements of Rowland and White[20] (red squares).

Keeping in mind that c_{ij}^S should be greater than c_{ij}^T (except for c_{44} since pure torsion involves no change in volume) and that our numerical uncertainty is around 10 GPa (see Appendix), the trend of the temperature dependence for each c_{ij} is in agreement with experimental data.

The pressure derivatives at RT given by our EOS and our elastic constant c_{ij}^T are $dc_{ij}/dp = 6 \pm 1$, 7.6 ± 1, 2.2 ± 1, 1.7 ± 1, and 0.6 ± 1 for c_{11}, c_{33}, c_{44}, c_{12}, and c_{13}, respectively, compare well with measurements in Ref. 16 [dc_{ij}/dp =6.92(3), 8.98(3), 2.55(3), 2.76(3), and 3.3(1)] except perhaps for c_{13}.

Given the individual elastic constants, several averaging procedures exist to estimate the shear (G) and the bulk (K) moduli for a polycrystal. At least four definitions are among the most popular: the Reuss, Voigt, Voigt-Reuss-Hill (VRH), and Artman-Strikman formulas. The polycrystalline anisotropy ratio $A_{VRH}[(G_V - G_R)/(G_V + G_R)]$ for the hcp phase is nearly zero so the hcp phase is weakly sensitive to the procedure. On the other hand, A_{VRH} for bcc varies between 0.18 and 0.48 as function of the volume[22] and thus the choice of the averaging procedure will influence the value of G for the bcc structure. We choose here the VRH formula which is suitable for the hcp phase of beryllium.[18,20]

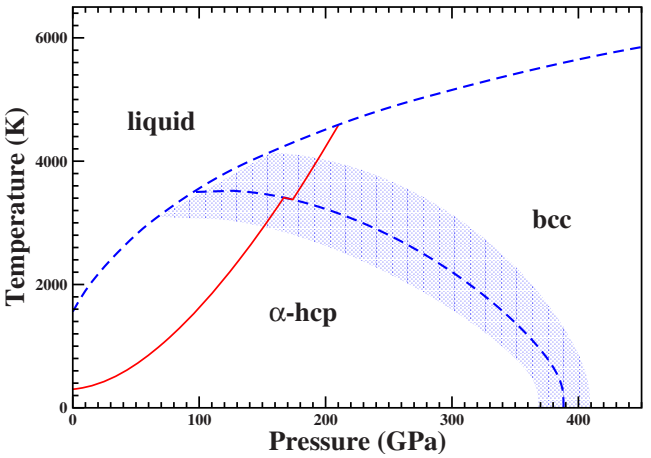

FIG. 8. (Color online) Theoretical (dashed lines) phase diagram of Be obtained by fit from our QHA calculations (see tables and text). The blue part between hcp and bcc phases reproduces uncertainties in the determination of line of the phase transition (see text). Red solid line is the Hugoniot curve up to its intersection with the melt line.

The temperature behavior of the shear modulus along eight isochors is shown in Fig. 10 (symbols). As usual, two regimes appear in temperature: nonlinear below the Debye temperature (i.e., approximately 1000 K) and linear above.

To fit our calculations, we propose to use an analytic form for the shear modulus as a function of density and temperature derived from the Burakovsky and Preston[43] formula modified according to Wachtman *et al.*[48] to take into account the nonlinear behavior below the Debye temperature.

$$G(\rho,T) = G(\rho,0)\{1 - b(\rho)[T/T_m(\rho)]\exp[-T_0(\rho)/T]\}. \tag{14}$$

$T_m(\rho)$ is defined by our melting line [Eq. (7) and Table I].

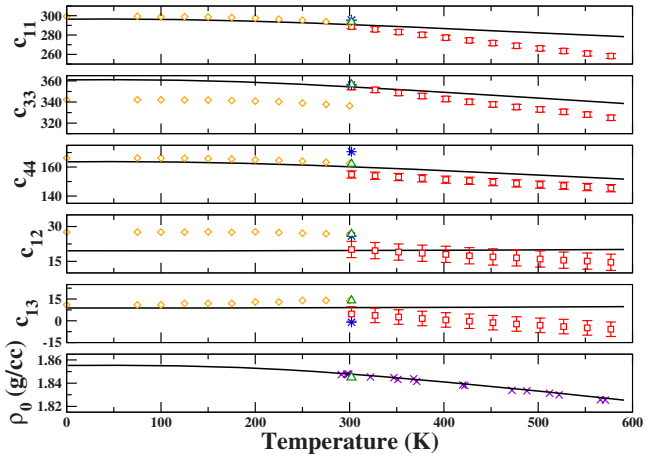

FIG. 9. (Color online) Theoretical c_{ij}^T (GPa) and density (in g/cc) versus temperature along the 1 bar isobar. Diamonds (Ref. 19), stars (Ref. 16), triangles up (Ref. 18), and squares (Ref. 20) are experimental c_{ij}^S and crosses experimental thermal-expansion data.[47]

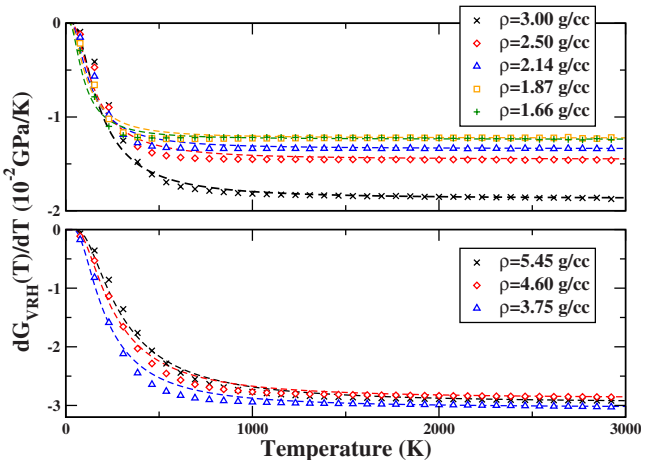

FIG. 10. (Color online) Evolution of dG_{VRH}/dT in function of temperature obtained by *ab initio* calculations (symbols) and from Eq. (14) (lines). Upper graph stands for the hcp phase and lower stands for the bcc phase.

The first term is

$$G(\rho,0) = G(\rho_0)\left(\frac{\rho}{\rho_0}\right)^{4/3} \exp\left[-6\gamma_1(\rho^{-1/3} - \rho_0^{-1/3}) - \frac{2\gamma_2}{q}(\rho^{-q} - \rho_0^{-q})\right]. \quad (15)$$

γ_1 is in $(\mathrm{g/cc})^{1/3}$ and γ_2 is in $(\mathrm{g/cc})^q$. q is without unit.

The second term in Eq. (14) is obtained from the asymptotic limit at high temperature of $dG(\rho,T)/dT$ deduced from Fig. 10. We observe that $b(\rho)$ can be approached by a simple linear expression: $b(\rho) \approx b_0 + b_1\rho \cdot b_0$ is without unit and b_1 in $(\mathrm{g/cc})^{-1}$.

The third term is adjusted by fitting the data: $T_0(\rho) = 0.2\theta_0(\rho) \cdot \theta_0$ is given by Eq. (12) and Tables III and IV. This value is relatively close to $\theta_0/3$ given in Ref. 33 as a standard value.

For the two phases, the coefficients are provided in Table V.[49]

B. Comparison with experiments

The adiabatic polycrystalline VRH shear modulus $G(T)$ along the ambient pressure isobar obtained with different approaches is reproduced in Fig. 11 by (1) a dashed line when only the effect of the thermal expansion predicted by our EOS is used. (2) A full line when we take into account the whole temperature dependence as expressed in formula (14).

TABLE V. Coefficients for Eqs. (14) and (15) for the shear modulus at $T=0$ K.

	hcp	bcc
ρ_0 (g/cc)	1.889	1.918
$G(\rho_0)$ (Gpa)	157.9	101.8
γ_1	−3.8328	0.1009
γ_2	4.5347	3.5927
q	0.4933	2.4902
b_0	0.012	0.59
b_1	0.075	−0.062

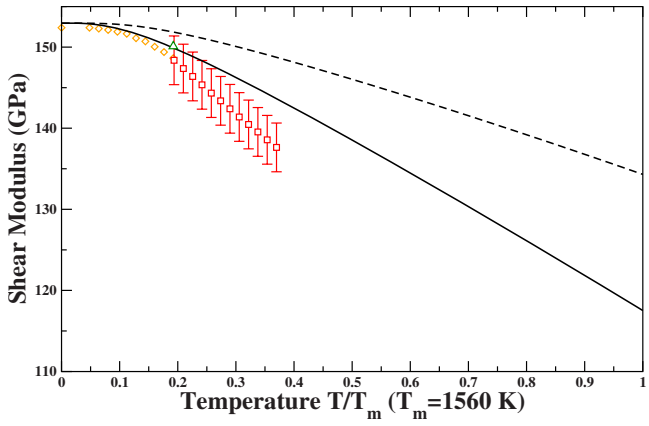

FIG. 11. (Color online) Shear modulus along the 1 bar isobar, as obtained in this work (full line). The *ab initio* shear modulus obtained using only the thermal expansion predicted by our EOS is reproduced by the dashed line. Diamonds (Ref. 19), triangle up (Ref. 18), and squares (Ref. 20) reproduced VRH adiabatic modulus obtained from experimental c_{ij}.

Comparisons are presented with moduli deduced from experimental elastic constants measured by Refs. 18–20 (symbols).

Exploiting the explicit temperature dependence leads to a better agreement with all experimental data.[18–20] Figure 12 shows the adiabatic polycrystalline VRH bulk modulus along the ambient pressure isobar given by our EOS and values deduced from elastic constants obtained by Refs. 19 and 20. At RT-RP, both bulk moduli, either the value obtained from the VRH average of our elastic constants or the value derived from our EOS, agree very well with the most recent experiments[18] and relatively well with Ref. 20.

However, the temperature dependence of the bulk modulus that we calculate is very different from Rowland and

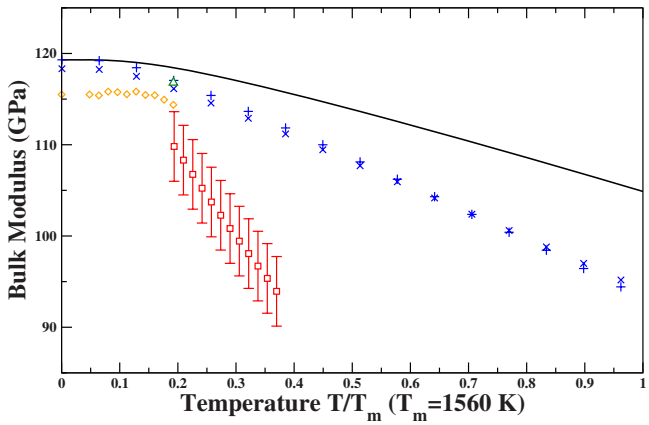

FIG. 12. (Color online) Full line: adiabatic bulk modulus along 1 bar isobar from our EOS. Plus and crosses reproduce isothermal bulk modulus deduced from elastic constant and EOS, respectively. Diamonds (Ref. 19), squares (Ref. 20), triangle up (Ref. 18) reproduce VRH adiabatic modulus obtained from experimental $c_{\mathrm{ij}}^{\mathrm{S}}$.

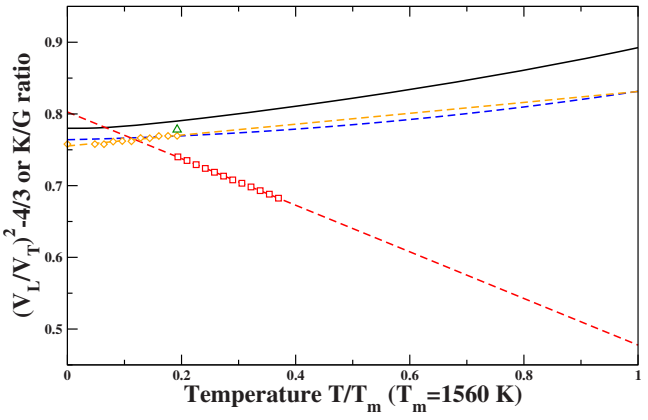

FIG. 13. (Color online) Ratio of the bulk over shear moduli obtained with our model (black line), compared to experimental data by Nadal and Bourgeois (Ref. 50) fit (blue dashed line), from Rowland and White (Ref. 20) (red dashed line), and Smith and Arbogast (Ref. 19) (orange dashed line) measurements (and extrapolations).

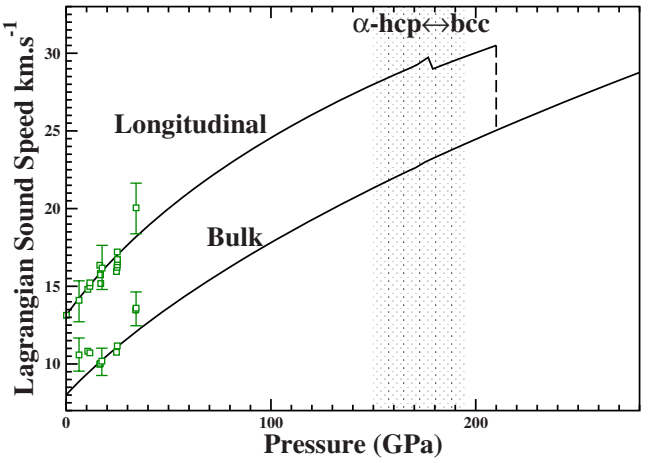

FIG. 14. (Color online) The adiabatic Lagrangian sound speeds on the main Hugoniot for the longitudinal and bulk mode (full line) compared to experiment (square: Ref. 51). The Eulerian sound speeds given in Ref. 51 are transformed into Lagrangian sound speed using the compression given by our EOS.

White experiments.[20] Along the 1 bar isobar, our $G(T)$ matches quite well Rowland and White experimental data whereas our $K(T)$ shows a large discrepancy with them.

A possible explanation is the following. In our calculations, VRH averaged bulk and shear moduli involve different sets of elastic constants, some of which could be wrong, being very sensitive to the convergence of the calculations. However, the good agreement between the isothermal bulk moduli calculated from elastic constants or derived from our EOS is an indication of the consistency of our calculations (cross and plus in Fig. 12) and the 300 K hcp isotherm matches well most recent diamond anvil cell measurements.

On the other hand, it could be that the experimental data are questionable. In order to bring a first element of response to this point, we take benefit of the preliminary results that Nadal and Bourgeois[50] have provided to us prior to publication. We extract a fit of the ratio of the longitudinal (V_L) over the transversal (V_T) sound velocities that they obtained from ultrasonic measurements on polycrystalline beryllium powders in the 300 to 1000 K temperature range (Fig. 13).

A direct comparison between this ratio and the theoretical K over G ratio can be made:

$$\frac{K}{G} = \left(\frac{V_L}{V_T}\right)^2 - \frac{4}{3}. \tag{16}$$

Figure 12 presents this ratio as obtained with our model (black line) compared to Rowland and White[20] (red dashed line) and Smith and Arbogast[19] (orange dashed line) measurements (extrapolated) and to new experimental data fitted by Nadal and Bourgeois[50] (blue dashed line).

The overall agreement between our work, Nadal and Bourgeois and Smith and Arbogast data strongly indicate that Rowland and White data along isobar may be questioned (particularly the combination of c_{ij} which leads to bulk modulus). Concerning data under dynamic loading, experimental data on bulk and longitudinal sound speeds on the principal Hugoniot are also available.[51] They are displayed in Fig. 14, together with the predicted Lagrangian sound speed given by our model.

We have already shown[25] that the hcp EOS accurately reproduces available shock Hugoniot data.[15,52–55] According to our EOS, the main Hugoniot intersects the hcp-bcc transition line at 180 GPa and 3500 K and crosses the melt curve above 210 GPa and 4500 K, close to the hcp-bcc phase boundary (Fig. 8).

Both longitudinal and bulk sound speeds are consistent with experiment.[51] The bulk sound speed is not sensitive to crystallographic changes whereas the longitudinal sound speed shows discontinuities. The location of the first slight discontinuity corresponds to the hcp↔bcc phase transition. The shaded zone marks the fact that its location can vary with the numerical approximations (uncertainty on Debye characteristic temperatures and cold curve). As the study of the behavior of the shear modulus along the solid-liquid line is out of the scope of this paper, G is arbitrarily set to zero above melting temperature (dashed line).

VI. CONCLUSION

We have investigated in details the phase diagram and the elastic constants of beryllium. We have carefully studied and discussed the behavior in density of the moments of the phonon densities of state to build an accurate multiphase EOS for the hcp and the bcc phases within a quasiharmonic approximation. The presence of a bcc pocket at low pressure and high temperature in the phase diagram and never predicted in QHA has also been addressed. We have shown that the negative frequencies of the T_1 phonon mode at N point shift to positive frequencies with increasing temperature, in a range consistent with the experimental phase diagram. This points out that anharmonicity should play the major role in stabilizing the bcc phase in this regime. Its thermodynamic stability has still to be proven.

TABLE VI. Distortion, energy expressions (in Voigt notation), and calculation parameters for the hcp structure. V_p is the volume prior to deformation.

Distortion	$\Delta E/V_p$ to $O(\delta^2)$	**k**-point grid	**q**-point grid
$\varepsilon_1=\delta$	$-p\delta+1/2c_{11}\delta^2$	$18\times18\times18$	$6\times6\times6$ (52 **q** points)
$\varepsilon_3=\delta$	$-p\delta+1/2c_{33}\delta^2$	$16\times16\times16$	$8\times8\times8$ (50 **q** points)
$\varepsilon_5=\delta$	$2[1/2p+c_{44}]\delta^2$	$18\times18\times18$	$6\times6\times6$ (68 **q** points)
$\varepsilon_1=\varepsilon_2=\delta$	$-2p\delta+[-p+c_{11}+c_{12}]\delta^2$	$16\times16\times16$	$8\times8\times8$ (50 **q** points)
$\varepsilon_1=\varepsilon_3=\delta$	$-2p\delta+0.5[-2p+c_{11}+2c_{13}+c_{33}]\delta^2$	$18\times18\times18$	$6\times6\times6$ (52 **q** points)

As for strength, we have also obtained the evolution of the Voigt-Reuss-Hill shear modulus with density and temperature from elastic constants within density-functional perturbation theory.

All our data (EOS and moduli) have been provided in an analytic form suitable for hydrocodes. Throughout the paper, our results are in very good agreement with most experimental data. However, new experiments would be interesting, first of all to revisit the phase diagram even at low pressure, in order to fix the transition lines and to consolidate the dependence of the bulk modulus and individual elastic constants in temperature.

ACKNOWLEDGMENTS

We gratefully thank M. H. Nadal and L. Bourgeois for communicating new experimental results prior to publication and for fruitful discussions.

APPENDIX

All calculations have been performed with AbInit package.[56] Our basis set included plane waves up to a kinetic-energy cutoff of 5000 eV. Sums over occupied electronic states were performed using the cold smearing method of Marzari[57] with $a=-0.5634$ and a smearing width of $\sigma=0.55$ eV. We have used a norm-conserving Hartwigsen, Goedecker, and Hutter pseudopotential which includes four electrons in the valence[58] within the generalized gradient approximations.[59] Reciprocal space sampling was performed with k-point grids of $20\times20\times20$ and $16\times16\times16$ for bcc and hcp structures respectively with a usual Monkhorst-Pack sampling (2 k points shift for bcc: $\pm1/4$; $\pm1/4$; $\pm1/4$ and one k-point shift for hcp: 0; 0; 0.5).

To evaluate the sensitivity of the density below which the bcc lattice becomes unstable, we carried out calculations using the frozen phonon method[41] with two codes: VASP (cms.mpi.univie.ac.at) and FP-LAPW (www.wien2k.at). The density is always in the vicinity of 2.1 g/cc whatever the ***k***-point integration (Gaussian, tetrahedron, or Fermi smearing with methods). As for elastic constants calculations or c/a ratio, we have verified that their values are insensitive (within the uncertainties that we provide below) to k-point integration smearing (we have checked Fermi smearing with electronic temperatures ranging from 300 to 3000 K).

For all phases, we have calculated ground-state energies, phonon-dispersion relations, and densities of states for 21 densities ranging from 1.4 to 6 g/cc. For the hcp phase, the optimization of the c/a ratio was performed at each volume. For the hcp and bcc phases, the equilibrium densities calculated are, respectively, 1.889 and 1.918 g/cc.

Within DFPT, the perturbation on the electron density created by a small displacement vector **u** around the equilibrium positions is associated to a phonon vector **q**. From a set of lattice distortions on the first Brillouin zone and using Fourier interpolation from this **q** grid, the full dynamical matrix is obtained.

For the phonon-dispersion relations, we used $47(10\times10\times10)$ and $50(8\times8\times8)$ **q** points for bcc and hcp phases, respectively, and $56(8\times8\times4)$ for α-Sm structure.

For distorted structures, we used the same parameters, except for **k**- and **q**-point grids. Distortions and corresponding parameters are reported in Tables VI and VII. In the ground state, individual elastic constants were calculated for the same 21 densities already defined above (ranging from 1.4 to 6 g/cc). In temperature, calculations are more expensive, so we calculated $c_{ij}(\rho,T)$ at three densities for the bcc structure (5.45, 4.6, and 3.75 g/cc) and five densities for the hcp structure (3, 2.5, 2.14, 1.87, and 1.66 g/cc).

As shown in Ref. 25, c/a ratio varies strongly with density. When dealing with equation of state and elastic properties, it could be that the c/a ratio would change with temperature due to anisotropic dilatation. In order to check this, we have calculated phonon-dispersion relations while changing the c/a ratio obtained in the ground state by $\pm1\%$, 2%, and 5% for all studied volumes and determined the minimum of the Helmholtz free energy.

We found that the c/a ratio remains mainly unchanged whatever the temperature $[c/a(V,T)=c/a(V,0)][1\pm2.5\times10^{-6}$ T], i.e., a variation less than 1% at 2000 K). Therefore, we will consider that the c/a ratio obtained in the

TABLE VII. Distortion, energy expressions (Voigt notation), and calculation parameters for the bcc structure. V_p is the volume prior to deformation.

Distortion	$\Delta E/V_p$ to $O(\delta^2)$	**k**-point grid	**q**-point grid
$\varepsilon_1=\delta$	$-p\delta+1/2c_{11}\delta^2$	$18\times18\times18$	$8\times8\times8$ (72 **q** points)
$\varepsilon_1=-\varepsilon_2=\delta$; $\varepsilon_3=\delta^2/(1-\delta^2)$	$[c_{11}-c_{12}]\delta^2$	$16\times16\times16$	$8\times8\times8$ (95 **q** points)
$\varepsilon_3=\delta^2/(4-\delta^2)$; $\varepsilon_6=\delta/2$	$1/2c_{44}\delta^2$	$18\times18\times18$	$8\times8\times8$ (95 **q** points)

ground state is constant along an isochor. Thus, for hcp structure, the c/a ratio is relaxed once and for all in the ground state.

The internal relaxations which affect c_{11}, c_{66}, c_{44}, and c_{12} (in Voigt notation) have also been performed. Concerning Eq. (13), different orders for the fit have been tested and the difference between the data and the fit checked.

A fourth-order polynomial has been chosen[60] (this leads at most to a 1 meV/atom departure on energy). The quadratic form is unable to adjust correctly the energy better than 30 meV/atom and the sixth order[61,62] does not improve our best fit.

In the ground state, we have checked four more distortions in order to address the reliability of the strained energies obtained either by direct calculations or by combination of elastic constants. Addition of temperature dependence of elastic constants along isochors obtained by DFPT leads also to a complete agreement between bulk moduli [calculated from the EOS or Reuss isothermal bulk modulus $-Vdp/dV=[(s_{11}+s_{22}+s_{33})+2(s_{12}+s_{13}+s_{23})]^{-1}$ where $[s_{ij}]=[c_{ij}]^{-1}$ are elastic compliance] whatever the temperature. From these results, we estimate an error of 5% in our elastic constants up to 200 GPa and about 10 GPa above.

*gregory.robert@cea.fr

[1] J. M. Servas and E. Martinez in *Ninth International Conference on the Mechanical and Physical Behaviour of Materials under Dynamic Loading* (EDP Sciences, Les Ulis (France), 2009), p. 539.

[2] D. A. Young, *Phase Diagrams of the Elements* (University of California Press, Oxford, England, 1991).

[3] M. François and M. Contre, *Proc. Conférence Intern. Metallurgie du Beryllium*, Grenoble, 1965 (PUF, Paris, 1966), p. 201.

[4] C. W. F. T. Pistorius, in *Progress in Solid State Chemistry*, edited by J. O. Mc Caldin and G. Somorja (Pergamon, New York, 1976), Vol. 11, p. 11.

[5] V. M. Amonenko, V. Y. Ivanov, G. F. Tikhinskii, V. A. Finkels, and I. V. Shapagin, Fiz. Met. Metalloved. **12**, 865 (1961).

[6] A. J. Martin and A. Moore, J. Less-Common Met. **1**, 85 (1959).

[7] A. Abey, LLNL Report No. UCRL53567, 1984 (unpublished).

[8] L. C. Ming and M. H. Manghnani, J. Phys. F: Met. Phys. **14**, L1 (1984).

[9] V. Vijayakumar, B. K. Godwal, Y. K. Vohra, S. K. Sikka, and R. Chidambaram, J. Phys. F: Met. Phys. **14**, L65 (1984).

[10] R. L. Reichlin, Rev. Sci. Instrum. **54**, 1674 (1983).

[11] N. Velisavljevic, G. N. Chesnut, Y. K. Vohra, S. T. Weir, V. Malba, and J. Akella, Phys. Rev. B **65**, 172107 (2002).

[12] J. Nakano, J. Phys.: Condens. Matter **14**, 10569 (2002).

[13] W. J. Evans, M. J. Lipp, H. Cynn, C. S. Yoo, M. Somayazulu, D. Häusermann, G. Shen, and V. Prakapenka, Phys. Rev. B **72**, 094113 (2005).

[14] L. X. Benedict, T. Ogitsu, A. Trave, C. J. Wu, P. A. Sterne, and E. Schwegler, Phys. Rev. B **79**, 064106 (2009).

[15] J. L. Wise, L. C. Chhabildas, and J. R. Asay, *SWCM-1981*, AIP Conference Proceedings No. 78 (AIP, New York, 1982), p. 417; L. C. Chhabildas, J. R. Wise, and J. R. Asay, *SWCM-1981*, AIP Conference Proceedings No. 78 (AIP, New York, 1982), p. 422.

[16] D. J. Silversmith and B. J. Averbach, Phys. Rev. B **1**, 567 (1970).

[17] L. Gold, Phys. Rev. **77**, 390 (1950); L. Testardi and J. Condon, Phys. Rev. B **1**, 3928 (1970).

[18] A. Migliori, H. Ledbetter, D. J. Thomas, and T. W. Darling, J. Appl. Phys. **95**, 2436 (2004).

[19] J. F. Smith and C. L. Arbogast, J. Appl. Phys. **31**, 99 (1960).

[20] W. D. Rowland and J. S. White, J. Phys. F: Met. Phys. **2**, 231 (1972).

[21] Y. I. Kokovikhin, Strength Mater. **22**, 1616 (1990).

[22] K. Kádas, L. Vitos, B. Johansson, and J. Kollár, Phys. Rev. B **75**, 035132 (2007); K. Kádas, L. Vitos, R. Ahuja, B. Johansson, and J. Kollár, *ibid.* **76**, 235109 (2007).

[23] G. V. Sin'ko and N. A. Smirnov, Phys. Rev. B **71**, 214108 (2005).

[24] S. P. Rudin, M. D. Jones, and J. D. Johnson, in *20th AIRAPT Conference Proceeding*, Karlsruhe, 2005, edited by E. Dinjus and N. Dahmen (Forschungszentrum Karlsruhe, Germany, 2005), p. 58.

[25] G. Robert and A. Sollier, J. Phys. IV **134**, 257 (2006).

[26] G. Robert, A. Sollier, and Ph. Legrand, in *Shock Compression of Condensed Matter-2007*, AIP Conference Proceedings No 955, edited by Mark Elert, Michael D. Furnish, Ricky Chau, Neil Holmes, and Jeffrey Nguyen, (AIP, New York, 2007), p. 97.

[27] G. Robert, A. Sollier, and Ph. Legrand, in APS March Meeting, New Orleans, 2008 (unpublished).

[28] P. K. Lam, M. Y. Chou, and M. L. Cohen, J. Phys. C **17**, 2065 (1984).

[29] P. Carrier, J. F. Justo, and R. M. Wentzcovitch, Phys. Rev. B **78**, 144302 (2008).

[30] V. P. Dmitriev, A. Yu. Kuznetsov, D. Machon, H. P. Weber, and P. Tolédano, Europhys. Lett. **61**, 783 (2003).

[31] B. Palanivel, R. S. Rao, B. K. Godwal, and S. K. Sikka, J. Phys.: Condens. Matter **12**, 8831 (2000).

[32] R. Stedman, Z. Amilius, R. Pauli, and O. Sundin, J. Phys. F: Met. Phys. **6**, 157 (1976).

[33] G. Grimvall, *Thermophysical Properties of Materials* (Elsevier Science B.V., Amsterdam, The Netherlands, 1999).

[34] G. V. Sin'ko and N. A. Smirnov, J. Phys.: Condens. Matter **14**, 6989 (2002).

[35] O. Hunderi and H. P. Myers, J. Phys. F: Met. Phys. **4**, 1088 (1974).

[36] C. A. Swenson, J. Appl. Phys. **70**, 3046 (1991).

[37] G. Ahlers, Phys. Rev. **145**, 419 (1966).

[38] R. W. Hill and P. L. Smith, Phil. Mag. **44**, 636 (1953).

[39] E. S. R. Gopal, *Specific Heats at Low Temperatures* (Heywood Books, London, 1966).

[40] N. Gopi Krishna and D. B. Sirdeshmukh, Acta Crystallogr. A **54**, 513 (1998).

[41] We choose a supercell of two atoms with a primitive lattice vector $\boldsymbol{a}$ $[a_x=(-1/2a,1/2a,1/2a)$, $a_y=(1/2a,-1/2a,1/2a)$, $a_z=(a,a,0)]$. The atomic positions are given by $\pm[1/4(a,a,a)+\boldsymbol{u}]$, where $\boldsymbol{u}$ is a displacement vector $[\boldsymbol{u}=(\lambda a,-\lambda a,0)$ for T_1 branch].

[42] L. X. Benedict, A. Trave, C. J. Wu, T. Ogitsu, E. Schwegler, and P. A. Sterne, in *Shock Compression of Condensed Matter-2007*, edited by Mark Elert, Michael D. Furnish, Ricky Chau, Neil Holmes, and Jeffrey Nguyen, AIP Conference Proceedings No. 955 (AIP, New York, 2007).
[43] L. Burakovsky and D. L. Preston, J. Phys. Chem. Solids **65**, 1581 (2004).
[44] F. Cricchio, A. B. Belonoshko, L. Burakovsky, D. L. Preston, and R. Ahuja, Phys. Rev. B **73**, 140103(R) (2006).
[45] J. Bouchet, F. Bottin, G. Jomard, and G. Zérah, Phys. Rev. B **80**, 094102 (2009).
[46] T. H. K. Barron and M. L. Klein, Proc. Phys. Soc. **85**, 523 (1965).
[47] P. Gordon, J. Appl. Phys. **20**, 908 (1949); E. A. Owen and T. L. Richards, Phil. Mag. **22**, 310 (1936).
[48] J. B. Wachtman, W. E. Tefft, D. G. Lam, and C. S. Apstein, Phys. Rev. **122**, 1754 (1961).
[49] Small differences with our previous calculations in Ref. 25 come from the lack of zero-point correction and the relaxation of the internal degrees of freedom in strained hcp structure.
[50] M. H. Nadal and L. Bourgeois J. Appl. Phys. **108**, 033512 (2010).
[51] L. C. Chhabildas, J. L. Wise, and J. R. Asay, in *Shock Waves in Condensed Matter*, AIP Conference Proceedings No. 78, edited by W. J. Nellis, L. Seaman, and R. A. Graham (AIP, New York, 1982), p. 422.
[52] R. G. McQueen and S. P. March, LASL Report No. GMX-6-566, 1964 (unpublished).
[53] W. H. Isbell, F. H. Shipman, and A. H. Jones, General Motors Corp. Materials Science Laboratory Report No. MSL-68-13 (1968).
[54] S. P. Marsh, *LASL Shock Hugoniot Data* (California Press, Berkeley, 1980).
[55] J. M. Walsh, M. H. Rice, R. G. McQueen, and F. L. Yarger, Phys. Rev. **108**, 196 (1957).
[56] X. Gonze, J.-M. Beuken, R. Caracas, F. Detraux, M. Fuchs, G. M. Rignanese, L. Sindic, M. Verstraete, G. Zerah, F. Jollet, M. Torrent, A. Roy, M. Mikami, Ph. Ghosez, J. Y. Raty, and D. C. Allan, Comput. Mater. Sci. **25**, 478 (2002).
[57] N. Marzari, Ph.D. thesis, University of Cambridge, 1996.
[58] S. Goedecker, M. Teter, and R. J. Hemley, Phys. Rev. B **54**, 1703 (1996).
[59] J. P. Perdew, K. Burke, and M. Ernzerhof, Phys. Rev. Lett. **77**, 3865 (1996).
[60] M. J. Mehl, Phys. Rev. B **47**, 2493 (1993).
[61] R. Dovesi, in *Lecture Notes in Chemistry*, edited by R. Pisani (Springer, New York, 1996), Vol. 67, p. 179.
[62] V. Trinite, Ph.D. thesis, Polytechnique, France, 2006.